IEEE Access
Multidisciplinary ⋮ Rapid Review ⋮ Open Access Journal

Received July 14, 2019, accepted July 25, 2019, date of publication July 29, 2019, date of current version August 13, 2019.

Digital Object Identifier 10.1109/ACCESS.2019.2931867

Optical Orbital Angular Momentum Shift-Keying Communication Using Direct Demodulation

YING LI[1], CHAOFENG WANG[1], XIAOKE ZHANG[1], JUNMIN LIU[1], YANLIANG HE[1], JIANGNAN XIAO[2], YANXIA GAO[1], SHUQING CHEN[1], XIAOMIN ZHANG[3], AND DIANYUAN FAN[1]

[1]International Collaborative Laboratory of 2D Materials for Optoelectronics Science & Technology of Ministry of Education, Engineering Technology Research Center for 2D Material Information Function Devices and Systems of Guangdong Province, College of Physics and Optoelectronic Engineering, Shenzhen University, Shenzhen 518060, China
[2]Shanghai Key Laboratory of Modern Optical System, Terahertz Science Cooperative Innovation Center, School of Optical-Electrical Computer Engineering, Terahertz Technology Innovation Research Institute, University of Shanghai for Science and Technology, Shanghai 200093, China
[3]Laser Fusion Research Center, China Academy of Engineering Physics, Mianyang 621900, China

Corresponding author: Shuqing Chen (shuqingchen@szu.edu.cn)

This work was supported in part by the National Natural Science Foundation of China under Grant 61805149, Grant 61575127, and Grant 61571188, in part by the Guangdong Natural Science Foundation under Grant 2016A030310065, in part by the Program of Fundamental Research of Shenzhen Science and Technology Plan under Grant JCYJ20180507182035270, in part by the Foundation for Distinguished Young Talents in Higher Education of Guangdong under Grant 2015KTSCX124 and Grant 2015KQNCX146, in part by the Science and Technology Project of Shenzhen under Grant ZDSYS201707271014468, in part by the Educational Commission of Guangdong Province under Grant 2016KCXTD006, and in part by the International Collaborative Laboratory of 2D Materials for Optoelectronics Science and Technology, Shenzhen University, under Grant 2DMOST2018003.

ABSTRACT Orbital angular momentum (OAM) shift-keying (SK), which manifests as the rapid switching of OAM modes, is crucial but severely hampered for lacking effective demodulation techniques in OAM communication. In this paper, we propose and investigate a novel direct-demodulation method for the OAM-SK communication. After passing through a well-designed beam slit, the optical vortex beam will possess varying output energies associated with the OAM modes. Hence, splitting the optical vortex beam into two sub-beams and one of them passing through the slit, we can directly extract the OAM-SK signals from the energy ratios of the two sub-beams. The results show that the bit-error-rate (BER) of demodulated OAM-SK signals can reach 3.7×10^{-3} even under the influence of strong atmospheric turbulence with $C_n^2 = 3 \times 10^{-12}$ and misalignment of 1.8 mm. Encoding digital signals to OAM modes and amplitude of optical vortex beams simultaneously, we construct a novel multi-modulation format composed of 16 QAM-OFDM and OAM-SK signals, which is also demodulated with the BER of 10^{-5} at the optical signal-to-noise ratio (OSNR) of 18 dB. These demonstrate that the direct-demodulation method provides a feasible way to demodulate OAM-SK signals and may show potential in complex OAM modulation communications.

INDEX TERMS Free-space optical communication, optical vortices, optical modulation.

I. INTRODUCTION

Angular momentum, one of the fundamental physical quantities in both classical and quantum mechanics, comprises spin- and orbital angular momentum (OAM) [1], [2]. The light beam carrying OAM is known as optical vortex beam, and its helical phase wave-front can be characterized by an azimuthal phase factor of $\exp(il\theta)$, where l is the topological charge associated with OAM mode [2]–[14]. Theoretically, l can take any integer numbers, and the optical vortex beams with different OAM modes are mutually orthogonal, which make optical vortex beam considerable potential in optical communication for providing an additional degree of freedom [15]–[17]. OAM multiplexing and OAM shift-keying (OAM-SK) are two main mechanisms of OAMbased communication [18]–[25]. Multiplexing optical vortex beams can provide more data channels and significantly increase the capacity density [5]–[7]. An ultra-high-speed communication with a total transmission capacity of 8.16Tbit/s and spectral efficiency of 435bit/s/Hz was achieved by multiplexing fifty-two optical vortex beams [26]. And the signals, which are respectively loaded to two optical vortex beams, were successfully transmitted over 18km OAMfiber with the bit-rate of 8.4Tbit/s [21]. However, the OAM-SK, manifesting

The associate editor coordinating the review of this manuscript and approving it for publication was Ling Cheng.

as the rapid switching of OAM modes and showing great potential in improving modulation ability and confidentiality, is severely hampered for lacking effective mode detection methods [27].

Some research works on OAM-SK communication have been reported [28]–[33]. Spatial separation is the most common way to demodulate OAM-SK signals, which diffracts optical vortex beam to assigned diffraction orders for identification. However, this method will damage the signals during the separation process, and the demodulation speed is also frustrated low for the complexity of systems and extra recognition time. Some improved detection methods have been proposed [30]–[33], such as identifying OAM modes by a retrieved array of sidelobe-modulated optical vortices (SMOVs) [33] or complicated algorithms [31]–[33]. In addition, a modal decomposition technique has also been reported in [34]–[36], which seems to show excellent merit in OAM-SK communication, but it still relies on complicated algorithms. These methods may provide reliable solutions for detecting OAM modes, but the complexity of demodulation systems and the inability to detect the rapidly switched OAM modes make them difficult to apply to OAM-SK communications. It is an incredible challenge to demodulate OAM-SK signals by using hologram or complex measurements at such a high-speed. Meanwhile, the OAM-SK modulation is rarely combined with other dimensions of light beams, especially for intensity, because spatially separating optical vortex beams will severely degenerate the transmitted signals. Hence, it is also a problem to demodulate OAM-SK and other modulation signals simultaneously.

In this paper, we propose and investigate a direct-demodulation method for demodulating OAM-SK signals, which may provide an efficient way for high-speed OAM-SK communication. After passing through a well-designed beam slit, the optical vortex beams with different OAM modes will possess varying output energies. The beam carrying OAM-SK signals is split into two sub-beams, and one of which is filtered by the slit to make the output energy change with the OAM modes. Thus, the OAM-SK signals can be directly demodulated by calculating the energy ratio of the two sub-beams. Furthermore, we constructed a novel multi-modulation format composed of OAM-SK and 16 QAM-OFDM signals by modulating data to OAM modes and intensity of the optical vortex beam simultaneously. Both the signals of 16 QAM-OFDM and OAM-SK were well demodulated by using the direct-demodulation method. Atmospheric turbulence and misalignment, two main factors resulting in performance degradation of OAM communication [37], were also investigated in this work. The results show that the OAM-SK signals can be demodulated with the BER of 3.7×10^{-3} even under the strong atmospheric turbulence with $C_n^2 = 3 \times 10^{-12}$ and misalignment of $1.8mm$. And the 16 QAM-OFDM intensity and OAM-SK multi-modulation signals were also demodulated with the BER of 10^{-5} at the optical signal-tonoise ratio (OSNR) of 18dB

II. PRINCIPLE OF IDENTIFYING OAM MODES USING THE DIRECT-DEMODULATION METHOD

Laguerre-Gaussian (LG) beam is the most common optical vortex beams. Its electric field distribution at the distance of z in free space can be expressed as [38]:

$$LG_p^l = \left(\frac{w_0}{w(z)}\right)\left(\frac{\sqrt{2}r}{w(z)}\right)^{|l|} L_p^{|l|}\left(\frac{2r^2}{w^2(z)}\right) exp\left(\frac{-r^2}{w^2(z)}\right) \cdot exp\left(-i\frac{kr^2 z}{z(z^2+z_r^2)}\right) exp(i(2p+|l|+1) \cdot tan^{-1}\left(\frac{z}{z_r}\right)) exp(-il\varphi) exp(-ikz), \quad (1)$$

where l is the topological charge, p is the transverse radial mode number. φ and r are the unit vectors in the azimuthal and radial directions, respectively. k is the wavenumber, ω_0 is the beam waist, $\omega(z)$ is the radius of the beam at z, and $z_r = k\omega_0^2/2$ is the Rayleigh length.

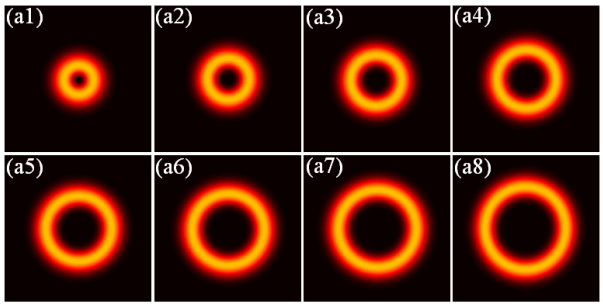

FIGURE 1. (a1)-(a8) The intensity distributions of the optical vortex beams with $l = 1$ to 8.

Figures 1(a1)-(a8) show the intensity distributions of the optical vortex beams ($l = 1$ to 8, $\lambda = 1.55 \times 10^{-6}m$) at far-field ($\omega_0$=$5 \times 10^{-4}m$, $z = 12m$). Because of the phase singularity at the beam cross-section, the intensity distribution of the optical vortex beam presents a 'doughnut' shape, and the diameter (circumference) of the intensity ring increases with the topological charge of $|l|$ (The ring diameter of $-l$ is numerically equal to l). Thus, equalizing the energy values of the optical vortex beams, we can directly identify the topological charge ($|l|$) from the energy per unit length of the ring.

The schematic diagram of identifying OAM modes based on the direct-demodulation method is illustrated in Fig. 2. The optical vortex beam is split into two sub-beams (L1, L2) by a beam splitter (BS), and its diameter increases with the transmission distance. One sub-beam (L1) transmits forwardly and maintains a 'doughnut' shape intensity distribution, whereas the other sub-beam (L2) is filtered by a fixed slit. The slit, truncating the 'doughnut' intensity distributions, has a size of $4mm$ in width and $20mm$ in length, as shown in Fig. 2(a). Then, two photo-detectors (PDs) are utilized to detect the energies. The energy ratio of the two sub-beams will vary with the topological charge, which provides a reference to identify OAM modes without any mode conversion.

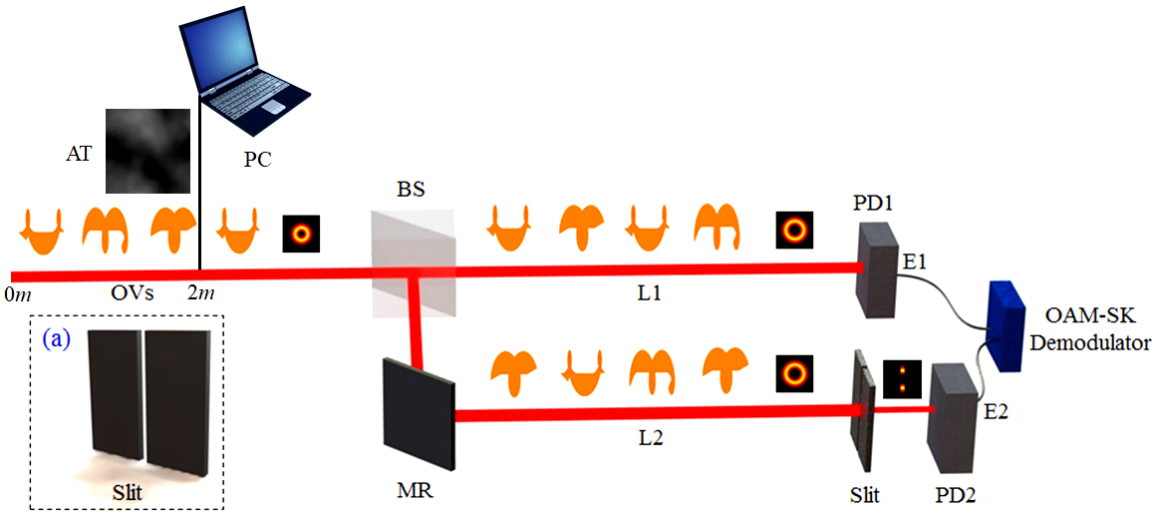

FIGURE 2. The schematic diagram of identifying OAM modes with the direct-demodulation method. BS: beam splitter; AT: atmospheric turbulence; PC: personal computer; MR: mirror; L1, L2: link 1, 2; PD: photo-detector; E1, E2: electrical signals.

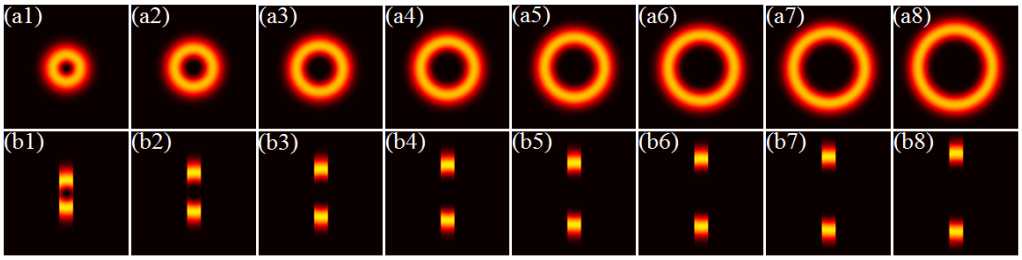

FIGURE 3. The intensity distributions of the sub-beams with different OAM modes. (a1)-(a8) L1 with $l = 1 - 8$, and (b1)-(b8) L2 with the topological charges corresponding to (a1)-(a8).

As described in the figure, the turbulence phase screen can be set at the initial position of $z_0 = 2m$.

Figures 3(a1)-(a8) present the intensity distributions of L1 with $l = 1$ to 8 at far-field ($z = 12m$). The energy values of these eight optical vortex beams are maintained, but the intensity diameters increase gradually with the topological charges of L1, so the energy per unit length of the ring decreases with the increase of topological charge. Figures 3(b1)-(b8) show the intensity distributions of L2 with the topological charges corresponding to Figs. 3(a1)-(a8) which pass through the slit with the width of $4mm$. Consistent with our previous discussion, the diameter (circumference) of the ring varies with the topological charge

Therefore, the energy ratio of L1 and L2 can be calculated by the following formula:

$$R_{\mathrm{E}} = \frac{E_1}{E_2} \approx \frac{L_{\mathrm{total}}}{L_{\mathrm{arc}}}, \tag{2}$$

where R_{E} represents the energy ratio of the two sub-beams, E_1 is the energy of L1, and E_2 is the energy of L2. L_{total} is the circumference of the intensity ring, and L_{arc} is the arc length of L2 passing through the slit.

The trend chart corresponding to the standard energy ratio of the two sub-beams is presented in Fig. 4. Limited by the

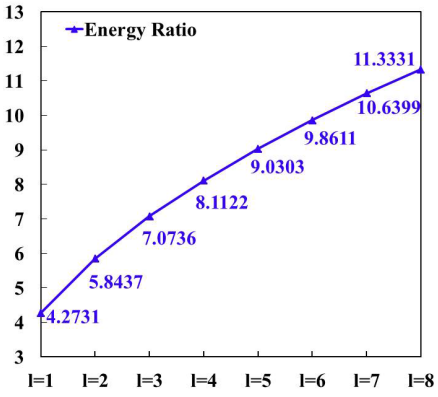

FIGURE 4. The curve corresponding to standard energy ratios (L1/L2) of the sub-beams with different OAM modes.

designed parameters, such as the waist of the beam ($\omega_0 = 5 \times 10^{-4}m$), the width ($4mm$) and length ($20mm$) of the beam slit, the size of receiving screen ($0.06m \times 0.06m$), and the initial position of z_0, the maximal OAM modes that this link can tolerate is $l = 8$. From the figure, the energy ratios increase from 4.2731 to 11.3331 for OAM modes with $l = 1$ to 8. According to the characteristic related to the energy

ratio, we can directly identify the OAM modes. And the energy ratio intervals of adjacent OAM modes also provide a decision reference which can resist noise attack to some extent.

III. THE INFLUENCE OF ATMOSPHERIC TURBULENCE AND MISALIGNMENT ON IDENTIFYING OAM MODES

A. THE INFLUENCE OF ATMOSPHERIC TURBULENCE

As one of the main factors leading to performance degradation in optical communications, atmospheric turbulence [39]–[41] causes intensity dispersion and helical-phase distortion [42], [43], which will destroy the mutual orthogonality among different OAM modes and result in OAM modes diffusion.

The famous structure function of the atmospheric refractive index, which obeys the "2/3 law", has been extensively studied since Kolmogorov and Obukhov proposed in 1941 [44]. It can be expressed as:

$$D_{\mathrm{n}}(r) = C_n^2 r^{2/3}, \quad l_0 \ll r \ll L_0, \tag{3}$$

where $D_{\mathrm{n}}(r)$ is the refractive index structure function. C_n^2 is the atmospheric refractive index structure constant [45], which acts as a crucial parameter for estimating the turbulence strength. r is the scale of atmospheric turbulence. l_0 stands for the inner scale, which describes that all turbulent eddy kinetic energy is converted into heat energy. L_0 is the outer scales and shows that the mean field transfers energy to turbulence. In frequency domain, the power spectral density of Kolmogorov spectrum is related to C_n^2, which can be expressed as:

$$\Phi_n(k) = 0.033 C_n^2 k^{-11/3}, \tag{4}$$

where k stands for the wave-number. However, this model is only available for the inertial region of $1L_0 \ll k \ll 1/l_0$. Furthermore, a Tatarskii power spectrum model [46] that can be suitable for the dissipation region is put forward, but there exists a singularity at $k = 0$ or $1/L_0 \to 0$ so that the authenticity of atmospheric turbulence cannot be completely simulated. Based on these problems existing in previous studies, a Hill-Andrews spectrum model is proposed [47]. The Hill-Andrews model and the turbulence phase screen used in this work can be described as follow:

$$\begin{aligned}\Phi_{\mathrm{n}}(\mathrm{k_x}, \mathrm{k_y}) = 0.033 C_{\mathrm{n}}^2 [1 + 1.802 \sqrt{\frac{k_{\mathrm{x}}^2 + k_{\mathrm{y}}^2}{k_l^2}} \\ -0.254 (\sqrt{\frac{k_x^2 + k_y^2}{k_l^2}})^{-7/12}] \\ \times exp(\frac{k_{\mathrm{x}}^2 + k_{\mathrm{y}}^2}{k_l^2}) (k_{\mathrm{x}}^2 + k_{\mathrm{y}}^2 + \frac{1}{L_0^2})^{-11/6},\end{aligned} \tag{5}$$

$$\phi(\mathrm{x,y}) = FFT[\mathrm{C} \cdot (2\pi/(N\Delta L)) \cdot \sqrt{2\pi k_0^2 \Delta \mathrm{z} \Phi_n(\mathrm{k_x}, \mathrm{k_y})}], \tag{6}$$

where $\Phi_n(k_x, k_y)$ represents the phase of k-space. k_{x} and k_{y} are the spatial frequency, $k_l = 3.3/l_0$. $\phi(\mathrm{x,y})$ is a $N \times N$ phase screen, and FFT represents two-dimensional (2-D) Fast Fourier Transform. ΔL represents the grid spacing of the phase screen, and Δz denotes the turbulence length.

If $\mathrm{U_0(x,y)}$ is the initial function of the beam ($z_0 = 2m$) uninfluenced by atmospheric turbulence, the propagation function $\mathrm{U(x,y)}$ after a transmission distance of Δz can be written as:

$$\begin{aligned}\mathrm{U(x,y)} \approx FFT^{-1}[FFT\{exp(i\phi(\mathrm{x,y}) \times \mathrm{U_0(x,y)}\} \\ \times exp(i(k_{\mathrm{x}}^2 + k_{\mathrm{y}}^2)\Delta \mathrm{z}/(2k))].\end{aligned} \tag{7}$$

Here, $exp(i(k_{\mathrm{x}}^2 + k_{\mathrm{y}}^2)\Delta z/(2k))$ is the Fresnel transfer function, FFT^{-1} is the 2-D Inverse Fast Fourier Transformation.

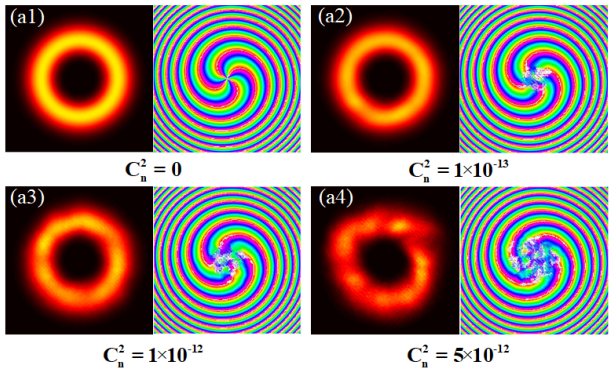

FIGURE 5. (a1)-(a4) The intensity distributions and corresponding helical phases of the optical vortex beams ($l = +4$, $z = 12m$) under the atmospheric turbulences with $C_n^2 = 0, 1 \times 10^{-13}, 1 \times 10^{-12}, 5 \times 10^{-12}$.

Under the influence of atmospheric turbulence, the refractive-index distribution in free space will become inhomogeneous, which makes the optical vortex beam propagate in a time-varying channel, and results in modes diffusions that manifests as the distortion in helical-phase wavefront and causes energy leakage to adjacent OAM channels. Figures 5(a1)-(a4) show the intensity distributions and corresponding helical phases of the optical vortex beam ($l = +4$, $z = 12m$) under the influence of turbulence strengths with $C_n^2 = 0, 1 \times 10^{-13}, 1 \times 10^{-12}, 5 \times 10^{-12}$, respectively. The wavelength of the optical vortex beam is $1.55 \times 10^6 m$, and the waist is $\omega_0 = 5 \times 10^{-4} m$. The turbulence phase screen is set with a size of $N \times N = 201 \times 201$. The grid spacing is $\Delta L = 2.5 \times 10^{-4} m$, and the inner and outer scales are $l_0 = 2 \times 10^{-4} m$ and $L_0 = 50m$, respectively. This screen is set at the position of $z_0 = 2m$ and the turbulence length is $\Delta z = 10m$. From the figures, the circular symmetry of the optical vortex beams are gradually destroyed, and the helical phase distortion increases with atmospheric turbulence strength because the OAM modes diffusion degree varies with the atmospheric refractive index structure constant C_n^2.

As described in Fig. 6, the fluctuation of turbulence becomes severe and causes serious modes diffusion in optical vortex beam ($l = +4$) with the increase of turbulence strength. Under the influence of atmospheric turbulence strengths with $C_n^2 = 1 \times 10^{-13}, 1 \times 10^{-12}, 5 \times 10^{-12}$,

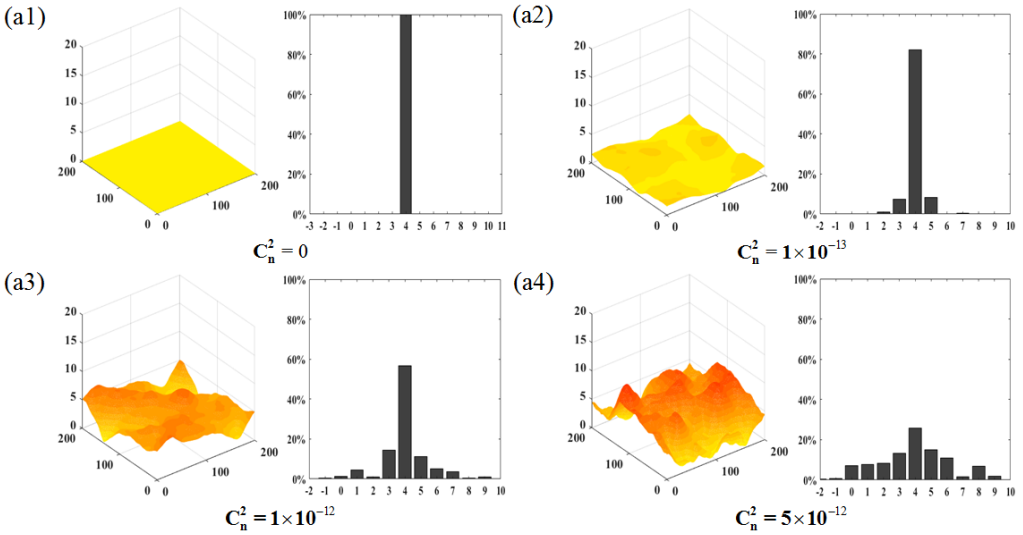

FIGURE 6. The OAM modes diffusion of the optical vortex beam ($l = +4$) influenced by atmospheric turbulence strengths of (a1) $C_n^2 = 0$, (a2) $C_n^2 = 1 \times 10^{-13}$, (a3) $C_n^2 = 1 \times 10^{-12}$, and (a4) $C_n^2 = 5 \times 10^{-12}$.

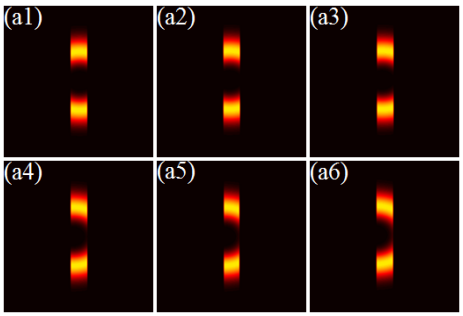

FIGURE 7. (a1)-(a6) The intensity distributions of the optical vortex beam ($l = 3$) passing through the slit with the misalignments of 0mm, 0.5mm, 1mm, 1.5mm, 2mm, 2.5mm.

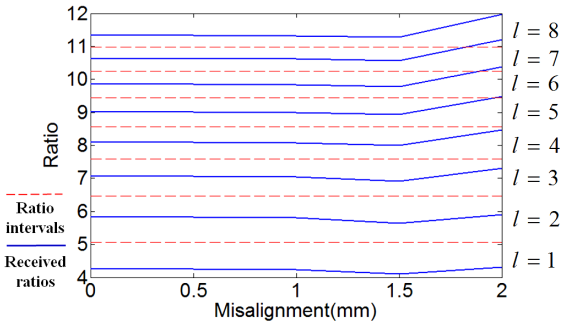

FIGURE 8. The received energy ratios of OAM modes of $l = 1$ to 8 as the function of misalignment.

the mode-diffusion makes the energy leak to adjacent OAM modes, which results that the OAM mode purity reduces to 80%, 55%, and 25%, respectively. This degeneration in OAM modes will seriously affect the accuracy of identification and lead to bit errors in communication. Hence, atmospheric turbulence is a factor that must be considered in optical communication, which causes modes diffusion and the decrease of the OSNR.

B. THE INFLUENCE OF MISALIGNMENT

Misalignment means the optical vortex beam deviates from the receiver, which also has a great influence on identification. Figures 7(a1)-(a6) describe the intensity distributions of the optical vortex beam ($l = 3$) passing through the slit ($4mm$ in width) with different misalignment. The intensity distribution without misalignment is shown in Fig. 7(a1). As presented in Figs. 7(a2)-(a6), with the misalignment of $0.5mm$, $1mm$, $1.5mm$, $2mm$, and $2.5mm$, the intensity distributions gradually deviate from the center. This deviation makes the detect energy changes and finally leads to a mutation in the energy ratio of the two sub-beams.

Figure 8 shows the energy ratios of L_{total}/L_{in} of the optical vortex beams ($l = 1$ to 8) with the atmospheric turbulence of $C_n^2 = 1 \times 10^{-12}$ and the misalignments of $0mm$, $0.5mm$, $1mm$, $1.5mm$, $2mm$. The ratio intervals are set to 5.5084, 6.4587, 7.5929, 8.5712, 9.4457, 10.251, 10.987 according to the reference ratios described in Fig. 4. From the figure, as the misalignment is less than $1.5mm$, the received ratios are well maintained. However, once the misalignment over $1.5mm$, the ratios increase rapidly, which will result in a misjudgment in identifying OAM modes if the received ratios exceed the ratio intervals, especially for the topological charges of $l = 5$ to 8. Therefore, the value of OAM modes that can be employed to perform OAM-SK communication is finite, but which should match the size of the beam slit. And the system performance and stability of OAM-SK communication link with higher OAM modes are worse than the one with lower OAM modes under the influence of misalignment.

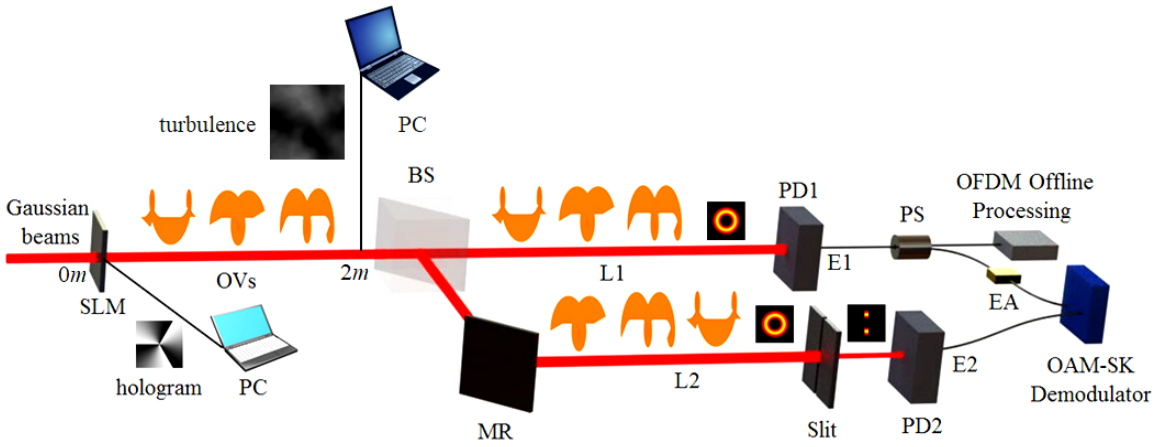

FIGURE 9. The schematic diagram of the OAM communication link based on direct-demodulation method. SLM: spatial light modulator; PC: personal computer; BS: beam splitter; PD: photo-detector; E1, E2: electrical signals detected by PD1, PD2; PS: power splitter; EA: electric amplifier.

IV. OAM COMMUNICATION LINK BASED ON THE DIRECT-DEMODULATION METHOD

Figure 9 shows the schematic diagram of the OAM communication link based on the direct-demodulation method. The SLM loaded with phase hologram was used to produce optical vortex beams, and the turbulence screen was added at the initial position of $z_0 = 2m$. For the multi-modulation, encoding signals to the intensity and OAM modes of beam simultaneously, the intensity-modulation signals can also be extracted by the direct-demodulation method. In this work, a BS was used to decompose the optical vortex beam into two sub-beams with the same energy. One sub-beam (L1) transmits forwardly without interference, while the other sub-beam (L2) was filtered by a well-designed slit ($4mm$ in width). Then, the OAM mode was directly identified by calculating the energy ratio (E1/E2) of the two sub-beams. By continuously refreshing the phase holograms, the produced optical vortex beam will possess switched OAM modes. Mapping the digital signals to the OAM modes (load different phase holograms), the OAM-SK modulation was realized. Furthermore, using a Gaussian beam carrying 16 QAM-OFDM signals as the input light, a multi-modulation communication link combining OAM-SK and 16 QAM-OFDM signals was achieved.

A. OAM-SK COMMUNICATION BASED ON THE DIRECT-DEMODULATION METHOD

The OAM-SK manifesting as the rapid switching of OAM modes was realized by encoding digital signals to OAM modes. Table 1 shows the mapping relationship between the OAM modes and encoded signals. Here, eight OAM modes were employed, and each OAM mode corresponds to a 3-bits binary series. To optimize the BER performance, we make the binary series among adjacent OAM modes only possess a 1-bit difference.

The energy ratios were divided into eight intervals by choosing the midpoints of adjacent ratios as the interval points, which acts as the decision thresholds for demodulating OAM-SK signals. Table 2 presents the relationship between the decoded data and decision thresholds.

TABLE 1. The energy ratios and encoded data for different OAM modes.

OAM (l)	Standard Ratios (L1/L2)	Encoded Data (Binary)
1	4.2731	000
2	5.8437	001
3	7.0736	010
4	8.1122	011
5	9.0303	100
6	9.8611	101
7	10.6399	110
8	11.3331	111

TABLE 2. The correspondence between decision thresholds and decoded data.

OAM (l)	Standard Ratios (L1/L2)	Decision Thresholds	Decode Data (Binary)
1	4.2731	0 ~ 5.5084	000
2	5.8437	5.5084 ~ 6.4587	001
3	7.0736	6.4587 ~ 7.5929	101
4	8.1122	7.5929 ~ 8.5712	100
5	9.0303	8.5712 ~ 9.4457	110
6	9.8611	9.4457 ~ 10.251	111
7	10.6399	10.251 ~ 10.987	011
8	11.3331	10.987 ~ ∞	010

The decision thresholds were well set for identifying OAM modes and can be applied to the OAM-SK communication links under the influence of misalignment and noise factors such as atmospheric turbulence, amplified spontaneous emission noise (ASE), and crosstalk.

The demodulation of OAM-SK signals was realized by directly extracting the energy ratios of the two sub-beams (L1, L2). The received ratios are compared with the ratio intervals for offline demodulation. As previously described, the output energy of the optical vortex beam filtered by the slit will be influenced by atmospheric turbulence and misalignment. Thus, we first investigate the effects of atmospheric turbulence on the demodulation of OAM-SK signals. Figure 10 illustrates the BER performance with the influence of atmospheric turbulence. From the BER curve, the OAM-SK signals are demodulated with a BER of 9.4×10^{-5} under the influence of moderate atmospheric turbulence ($C_n^2 < 0.5 \times 10^{-12}$). Even under the strong atmospheric turbulence of $C_n^2 = 3 \times 10^{-12}$, the BER also below 3.7×10^{-3}. The reason for the BER increases with the atmospheric turbulence strength can attribute to the beam spreading and scintillation.

TABLE 3. The received ratios of the optical vortex beams with the influence of misalignment.

OAM (l)	Received Energy Ratios					Decision Thresholds
	0*mm*	0.5*mm*	1*mm*	1.5*mm*	2*mm*	
1	4.27	4.25	4.23	4.10	4.34	0 ~ 5.5084
2	5.84	5.82	5.80	5.63	5.90	5.5084 ~ 6.4587
3	7.07	7.06	7.04	6.92	7.30	6.4587 ~ 7.5929
4	8.11	8.10	8.08	8.01	8.47	7.5929 ~ 8.5712
5	9.03	9.02	9.00	8.93	9.48	8.5712 ~ 9.4457
6	9.86	9.85	9.84	9.78	10.38	9.4457 ~ 10.251
7	10.63	10.63	10.62	10.56	11.21	10.251 ~ 10.987
8	11.33	11.33	11.32	11.27	11.98	10.987 ~ ∞

We have further studied the influence of misalignment on the BER performance under the strong atmospheric turbulence of $C_n^2 = 1 \times 10^{-12}$. As shown in Table 3, the received ratios slightly decrease with the misalignment under $\sim 1.5mm$. However, once the misalignment over $2mm$, the ratios rapidly raised, and the ratios corresponding to OAM modes of $l = 5$ to 8 exceed the decision threshold. These indicate that the misalignment has a greater impact on the detection of higher-order OAM modes, leading to a misjudgment in identifying OAM modes and deteriorating the BER performance of OAM-SK communication link.

Figure 11 shows the BER curve as the function of misalignment under the influence of atmospheric turbulence with $C_n^2 = 1 \times 10^{-12}$. The BER increases gradually with the misalignment below $1.8mm$, but still less than 9×10^{-4} at the misalignment of $1.8mm$. However, when the misalignment over $1.8mm$, the BER increases because the received ratios

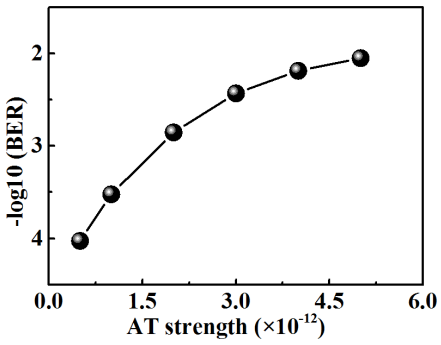

FIGURE 10. The BER curve as the function of atmospheric turbulence strength.

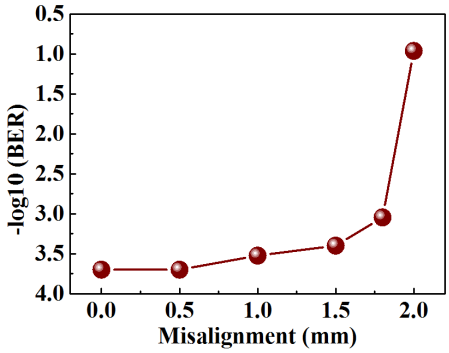

FIGURE 11. The BER curve as the function of misalignment.

corresponding to OAM modes (l=1 to 8) deviate the center and even exceed the decision thresholds, especially for the higher-order OAM modes.

B. OAM-SK AND 16 QAM-OFDM MULTI-MODULATION COMMUNICATION BASED ON DIRECT-DEMODULATION

The OAM-SK and 16 QAM-OFDM multi-modulation communication based on the direct-demodulation method was realized by modulating 16 QAM-OFDM signals to the Gaussian input beam, as shown in Fig. 9. Here, the 16 QAM-OFDM signals should be transmitted in a fixed time-slot to avoid being damaged because there is a transition state existed in the refresh process of the two adjacent OAM modes. After propagating for a certain distance in free optical space, the optical vortex beam carrying OAM-SK and 16 QAM-OFDM signals were divided into two sub-beams (L1, L2) by a BS. The L1 propagates forwardly while the other sub-beam (L2) was filtered by a slit ($4mm$in width) before being converted into electrical signals (E1, E2) by PD1 and PD2, respectively. The E1 was divided by a power splitter (PS, 50% : 50%), one of which was amplified by an electrical amplifier (EA) and combined with E2 for demodulating OAM-SK signals, and the other was used for the off-line processing of 16 QAM-OFDM signals.

Figure 12 shows the BER performance of the OAM-SK signals with the influence of atmospheric turbulence in the multi-modulation communication link. The BER of the

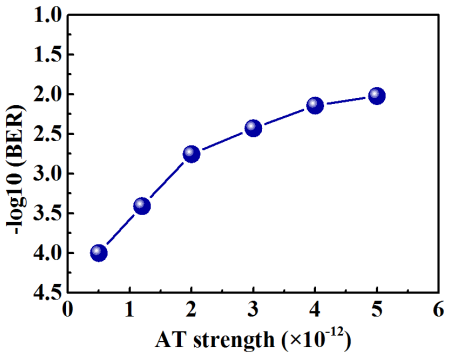

FIGURE 12. The BER curve as the function of atmospheric turbulence strength in the multi-modulation communication link.

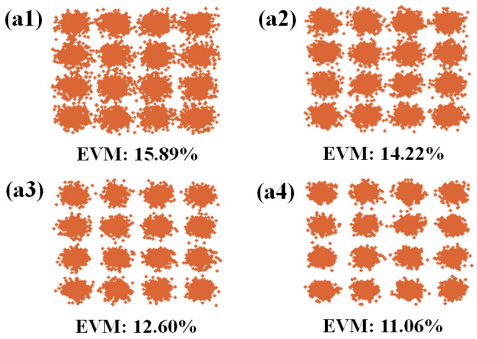

FIGURE 13. The constellations of 16 QAM-OFDM signals at the OSNR of (a) 15dB, (b) 16dB, (c) 17dB, and (d) 18dB.

demodulated OAM-SK signals is 9.8×10^{-5} with the atmospheric turbulence of $C_n^2 = 0.5 \times 10^{-12}$, and can still reach 3.8×10^{-3} even under the influence of strong atmospheric turbulence with $C_n^2 = 3 \times 10^{-12}$.

The down-conversion of 16 QAM-OFDM signals in the multi-modulation communication link is also based on direct-demodulation. The influence of atmospheric turbulence on the optical vortex beam will lead to signal damage and optical energy spreading, which further results in the deterioration of communication performance. That is, atmospheric turbulence brings a decrease of OSNR to the multi-modulation communication link. With the atmospheric turbulence strength increases, the OSNR decreases and makes the convergence of demodulation constellations worse. Figures 13(a1)-(a4) describe the demodulated constellations and corresponding error vector magnitudes (EVMs) of the 16 QAM-OFDM signals at the OSNR of 15dB, 16dB, 17dB, 18dB, respectively. From the figures, with the OSNR decreased from 15dB to 18dB, the EVMs increased from 11.06% to 15.89%, but the constellations can still be distinguished.

Figure 14 shows the BER performance of the demodulated 16 QAM-OFDM signals under different OSNRs in the multi-modulation link. When the OSNR is 18dB, the 16 QAM-OFDM signals were demodulated with a BER of 1.5×10^{-5}. As the OSNR reduced to 15dB, the BER is still below 1.9×10^{-3}. These demonstrate that the direct-demodulation method for the demodulation of 16 QAM-OFDM signals is well performed in the designed multi-modulation communication link.

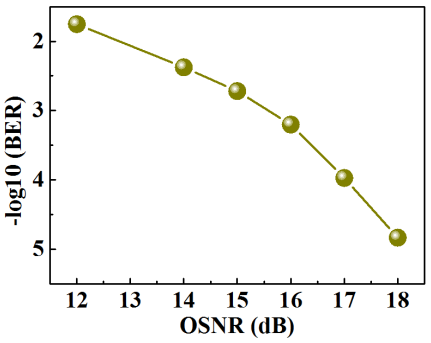

FIGURE 14. The BER-OSNR curve of 16 QAM-OFDM signals in the multi-modulation communication link.

V. DISCUSSION AND CONCLUSION

In this work, we propose and investigate a novel direct-demodulation method for demodulating OAM-SK signals, which is implemented with a well-designed beam slit. Splitting the optical vortex beam into two sub-beams and one of which passes through the slit, we can directly extract the OAM-SK signals from the energy ratios of the two sub-beams. This method can directly convert the OAM modes information into energy ratios without any mode conversion, making it possible to demodulate OAM-SK signals in high-speed. Besides, this technique is also suitable for identifying any ring-based modes, such as, the cylindrical vector beam [48] and the vector vortex beam [49], of which the diameter varies with the polarization order or OAM mode

In addition, it can directly demodulate multi-modulation signals composed of OAM-SK and OFDM intensity-modulation signals simultaneously because OAM is a dimension independent of the intensity of lights. Furthermore, this method has the advantage of mitigating atmospheric turbulence and misalignment bellow 1.8*mm* in OAM-SK communication because of the high tolerance of decision thresholds in resisting the adverse effects of atmospheric turbulence- and misalignment-induced. The results show that the BER is less than 3.8×10^{-3} even under the strong atmospheric turbulence of $C_n^2 = 1 \times 10^{-12}$ and the misalignment of 1.8*mm* in OAM-SK communication link. And the 16 QAM-OFDM and OAM-SK signals were also well demodulated with the BER of 3.8×10^{-3} under the strong atmospheric turbulence of $C_n^2 = 1 \times 10^{-12}$. These results indicate that the direct-demodulation method may possess potential values in high-speed and complex OAM based modulation communications.

REFERENCES

[1] L. Mandel, E. Wolf, and J. H. Shapiro, "Optical coherence and quantum optics," *Phys. Today*, vol. 49, no. 5, pp. 68–70, 1996.
[2] N. Bozinovic, Y. Yue, Y. Ren, M. Tur, P. Kristensen, H. Huang, and S. Ramachandran, "Terabit-scale orbital angular momentum mode division multiplexing in fibers," *Science*, vol. 340, pp. 1545–1548, Jun. 2013.
[3] L. Allen, M. W. Beijersbergen, R. Spreeuw, and J. Woerdman, "Orbital angular momentum of light and the transformation of Laguerre–Gaussian laser modes," *Phys. Rev. A, Gen. Phys.*, vol. 45, no. 11, pp. 8185–8189, Jun. 1992.

[4] D. L. Andrews, *Structured Light and Its Applications: An Introduction to Phase-Structured Beams and Nanoscale Optical Forces*. New York, NY, USA: Academic, 2008.

[5] B. Guan, R. P. Scott, C. Qin, N. K. Fontaine, T. Su, C. Ferrari, M. Cappuzzo, F. Klemens, B. Keller, M. Earnshaw, and S. J. B. Yoo, "Free-space coherent optical communication with orbital angular, momentum multiplexing/demultiplexing using a hybrid 3D photonic integrated circuit," *Opt. Express*, vol. 22, no. 1, pp. 145–156, 2014.

[6] J. Wang, J.-Y. Yang, I. M. Fazal, N. Ahmed, Y. Yan, H. Huang, Y. Ren, Y. Yue, S. Dolinar, M. Tur, and A. E. Willner, "Terabit free-space data transmission employing orbital angular momentum multiplexing," *Nature Photon.*, vol. 6, pp. 488–496, Jun. 2012.

[7] H. Huang, G. Xie, Y. Yan, N. Ahmed, Y. Ren, Y. Yue, D. Rogawski, M. J. Willner, B. I. Erkmen, K. M. Birnbaum, S. J. Dolinar, M. P. J. Lavery, M. J. Padgett, M. Tur, and A. E. Willner, "100 Tbit/s free-space data link enabled by three-dimensional multiplexing of orbital angular momentum, polarization, and wavelength," *Opt. Lett.*, vol. 39, no. 2, pp. 197–200, 2014.

[8] R. C. Devlin, A. Ambrosio, D. Wintz, S. L. Oscurato, A. Y. Zhu, M. Khorasaninejad, J. Oh, P. Maddalena, and F. Capasso, "Spin-to-orbital angular momentum conversion in dielectric metasurfaces: Erratum," *Opt. Express*, vol. 25, no. 1, pp. 377–393, 2017.

[9] A. E. Willner, H. Huang, Y. Yan, Y. Ren, N. Ahmed, G. Xie, C. Bao, L. Li, Y. Cao, Z. Zhao, J. Wang, M. P. J. Lavery, M. Tur, S. Ramachandran, A. F. Molisch, N. Ashrafi, and S. Ashrafi, "Optical communications using orbital angular momentum beams," *Adv. Opt. Photon.*, vol. 7, pp. 66–106, Mar. 2015.

[10] Y. Yan, G. Xie, M. P. J. Lavery, H. Huang, N. Ahmed, C. Bao, Y. Ren, Y. Cao, L. Li, Z. Zhao, A. F. Molisch, M. Tur, M. J. Padgett, and A. E. Willner, "High-capacity millimetre-wave communications with orbital angular momentum multiplexing," *Nature Commun.*, vol. 5, Sep. 2014, Art. no. 4876.

[11] P. Martelli, A. Gatto, P. Boffi, and M. Martinelli, "Free-space optical transmission with orbital angular momentum division multiplexing," *Electron. Lett.*, vol. 47, no. 17, pp. 972–973, Aug. 2011.

[12] Y. He, H. Ye, J. Liu, Z. Xie, X. Zhang, Y. Xiang, S. Chen, Y. Li, and D. Fan, "Order-controllable cylindrical vector vortex beam generation by using spatial light modulator and cascaded metasurfaces," *IEEE Photon. J.*, vol. 9, no. 5, Oct. 2017, Art. no. 6101710.

[13] X. Zhang, Y. He, Y. Cai, M. Su, X. Zhou, Y. Chen, S. Chen, Y. Xiang, L. Chen, C. Su, Y. Li, and D. Fan, "Coherent separation detection for orbital angular momentum multiplexing in free-space optical communications," *IEEE Photon. J.*, vol. 9, no. 3, Jun. 2017, Art. no. 7903811.

[14] Y. He, Y. Li, J. Liu, X. Zhang, Y. Cai, Y. Chen, S. Chen, and D. Fan, "Switchable phase and polarization singular beams generation using dielectric metasurfaces," *Sci. Rep.*, vol. 7, no. 1, 2017, Art. no. 6814.

[15] F. Wen, I. Ali, A. Hasan, C. Li, H. Tang, Y. Zhang, and Y. Zhang, "Ultrafast optical transistor and router of multi-order fluorescence and spontaneous parametric four-wave mixing in Pr^{3+}:YSO," *Opt. Lett.*, vol. 40, no. 20, pp. 4599–4602, 2015.

[16] G. Vallone, V. D'Ambrosio, A. Sponselli, S. Slussarenko, L. Marrucci, F. Sciarrino, and P. Villoresi, "Free-space quantum key distribution by rotation-invariant twisted photons," *Phys. Rev. Lett.*, vol. 113, no. 6, 2014, Art. no. 060503.

[17] F. Wen, Z. Li, Y. Zhang, H. Gao, J. Che, J. Che, H. Abdulkhaleq, Y. Zhang, and H. Wang, "Triple-mode squeezing with dressed six-wave mixing," *Sci. Rep.*, vol. 6, no. 1, 2016, Art. no. 25554.

[18] T. Lei, M. Zhang, Y. Li, P. Jia, G. N. Liu, X. Xu, Z. Li, C. Min, J. Lin, C. Yu, H. Niu, and X. Yuan, "Massive individual orbital angular momentum channels for multiplexing enabled by Dammann gratings," *Light Sci. App.*, vol. 4, no. 3, 2015, Art. no. e257.

[19] H. Huang, G. Xie, Y. Yan, N. Ahmed, Y. Ren, Y. Yue, D. Rogawski, M. J. Willner, B. I. Erkmen, K. M. Birnbaum, S. J. Dolinar, M. P. J. Lavery, M. J. Padgett, M. Tur, and A. E. Willner, "100 Tbit/s free-space data link enabled by three-dimensional multiplexing of orbital angular momentum, polarization, and wavelength," *Opt. Lett.*, vol. 39, no. 2, pp. 197–200, 2014.

[20] Y. Yan, Y. Yue, H. Huang, Y. Ren, N. Ahmed, M. Tur, S. Dolinar, and A. Willner, "Multicasting in a spatial division multiplexing system based on optical orbital angular momentum," *Opt. Lett.*, vol. 38, no. 19, pp. 3930–3933, 2013.

[21] L. Zhu, G. Zhu, A. Wang, L. Wang, J. Ai, S. Chen, C. Du, J. Liu, S. Yu, and J. Wang, "18 km low-crosstalk OAM+WDM transmission with 224 individual channels enabled by a ring-core fiber with large high-order mode group separation," *Opt. Lett.*, vol. 43, no. 8, pp. 1890–1893, 2018.

[22] J. Liu and J. Wang, "Polarization-insensitive PAM-4-carrying free-space orbital angular momentum (OAM) communications," *Opt. Express*, vol. 24, no. 4, pp. 4258–4269, 2016.

[23] H. Huang, G. Milione, M. P. J. Lavery, G. Xie, Y. Ren, Y. Cao, N. Ahmed, T. A. Nguyen, D. A. Nolan, M.-J. Li, M. Tur, R. R. Alfano, and A. E. Willner, "Mode division multiplexing using an orbital angular momentum mode sorter and MIMO-DSP over a graded-index few-mode optical fibre," *Sci. Rep.*, vol. 5, Oct. 2015, Art. no. 14931.

[24] Y. Fang, J. Yu, J. Zhang, N. Chi, J. Xiao, and G.-K. Chang, "Ultrahigh-capacity access network architecture for mobile data backhaul using integrated W-band wireless and free-space optical links with OAM multiplexing," *Opt. Lett.*, vol. 39, no. 14, pp. 4168–4171, 2014.

[25] Y. Fang, J. Yu, N. Chi, J. Zhang, and J. Xiao, "A novel PON architecture based on OAM multiplexing for efficient bandwidth utilization," *IEEE Photon. J.*, vol. 7, no. 1, pp. 1–6, Feb. 2015.

[26] J. Wang, J. Liu, X. Lv, L. Zhu, D. Wang, S. Li, A. Wang, Y. Zhao, Y. Long, J. Du, X. Hu, N. Zhou, S. Chen, L. Fang, and F. Zhang, "Ultra-high 435-bit/s/Hz spectral efficiency using N-dimentional multiplexing and modulation link with pol-muxed 52 orbital angular momentum (OAM) modes carrying Nyquist 32-QAM signals," in *Proc. Eur. Conf. Opt. Commun. (ECOC)*, Sep./Oct. 2015, pp. 1–3.

[27] S. Mi, T. Wang, G.-S. Jin, and C. Wang, "High-capacity quantum secure direct communication with orbital angular momentum of photons," *IEEE Photon. J.*, vol. 7, no. 5, Oct. 2015, Art. no. 7600108.

[28] G. Gibson, J. Courtial, M. J. Padgett, M. Vasnetsov, and V. Pas'ko, "Free-space information transfer using light beams carrying orbital angular momentum," *Opt. Express*, vol. 12, no. 22, pp. 5448–5456, 2004.

[29] R. Čelechovský and Z. Bouchal, "Optical implementation of the vortex information channel," *New J. Phys.*, vol. 9, no. 9, pp. 1–12, 2007.

[30] I. B. Djordjevic, "Deep-space and near-Earth optical communications by coded orbital angular momentum (OAM) modulation," *Opt. Express*, vol. 19, no. 15, pp. 14277–14289, Jul. 2011.

[31] C. Kai, P. Huang, F. Shen, H. Zhou, and Z. Guo, "Orbital angular momentum shift keying based optical communication system," *IEEE Photon. J.*, vol. 9, no. 2, Apr. 2017, Art. no. 7902510.

[32] L. Torner, J. P. Torres, and S. Carrasco, "Digital spiral imaging," *Opt. Express*, vol. 13, no. 3, pp. 873–881, 2005.

[33] P. Jia, Y. Yang, and X. Yuan, "Sidelobe-modulated optical vortices for free-space communication," *Opt. Lett.*, vol. 38, no. 4, pp. 588–590, 2013.

[34] C. Schulze, A. Dudley, D. Flamm, M. Duparré, and A. Forbes, "Measurement of the orbital angular momentum density of light by modal decomposition," *New J. Phy.*, vol. 15, no. 7, 2013, Art. no. 073025.

[35] J. Guo, D. Shi, Q. Wang, F. Pang, and Q. Liang, "A domain decomposition approach for static and dynamic analysis of composite laminated curved beam with general elastic restrains," *Mech. Adv. Mater. Struct.*, vol. 26, no. 16, pp. 1390–1402, 2019.

[36] K. Xie, W. Liu, Q. Zhou, L. Huang, Z. Jiang, F. Xi, and X. Xu, "Adaptive phase correction of dynamic multimode beam based on modal decomposition," *Opt. Express*, vol. 27, no. 10, pp. 13793–13802, 2019.

[37] W. Wang, P. Wang, T. Cao, H. Tian, Y. Zhang, and L. Guo, "Performance investigation of underwater wireless optical communication system using M -ary OAMSK modulation over oceanic turbulence," *IEEE Photon. J.*, vol. 9, no. 5, 2017, Art. no. 7905315.

[38] I. B. Djordjevic and M. Arabaci, "LDPC-coded orbital angular momentum (OAM) modulation for free-space optical communication," *Opt. Express*, vol. 18, no. 24, pp. 24722–24728, 2010.

[39] B. Rodenburg, M. P. J. Lavery, M. Malik, M. N. O'Sullivan, M. Mirhosseini, D. J. Robertson, M. Padgett, and R. W. Boyd, "Influence of atmospheric turbulence on states of light carrying orbital angular momentum," *Opt. Lett.*, vol. 37, no. 17, pp. 3735–3737, Sep. 2012.

[40] M. Malik, M. O'Sullivan, B. Rodenburg, M. Mirhosseini, J. Leach, M. P. J. Lavery, M. J. Padgett, and R. W. Boyd, "Influence of atmospheric turbulence on optical communications using orbital angular momentum for encoding," *Opt. Express*, vol. 20, no. 12, pp. 13195–13200, 2014.

[41] W. Cheng, J. W. Haus, and Q. Zhan, "Propagation of vector vortex beams through a turbulent atmosphere," *Opt. Express*, vol. 17, no. 20, pp. 17829–17836, 2009.

[42] C. Paterson, "Atmospheric turbulence and orbital angular momentum of single photons for optical communication," *Phys. Rev. Lett.*, vol. 94, no. 15, 2005, Art. no. 153901.

[43] G. A. Tyler and R. W. Boyd, "Influence of atmospheric turbulence on the propagation of quantum states of light carrying orbital angular momentum," *Opt. Lett.*, vol. 34, no. 2, pp. 142–144, Jan. 2009.

[44] A. N. Kolmogorov, "The local structure of turbulence in incompressible viscous fluid for very large Reynolds numbers," *Proc. Math. Phys. Sci.*, vol. 434, no. 1890, pp. 9–13, 1991.
[45] J. A. Anguita, M. A. Neifeld, and B. V. Vasic, "Turbulence-induced channel crosstalk in an orbital angular momentum-multiplexed free-space optical link," *Appl. Opt.*, vol. 47, no. 13, pp. 2414–2429, May 2008.
[46] X. Chu, "Evolution of an Airy beam in turbulence," *Opt. Lett.*, vol. 36, no. 14, pp. 2701–2703, 2011.
[47] L. C. Andrews and R. L. Phillips, *Laser Beam Propagation Through Random Media*, 2nd ed. Bellingham, WA, USA: SPIE, 2005.
[48] Q. Zhan, "Cylindrical vector beams: From mathematical concepts to applications," *Adv. Opt. Photon.*, vol. 1, no. 1, pp. 1–57, 2009.
[49] F. Yue, D. Wen, J. Xin, B. D. Gerardot, J. Li, and X. Chen, "Vector vortex beam generation with a single plasmonic metasurface," *ACS Photon.*, vol. 3, no. 9, pp. 1558–1563, 2016.

YING LI received the Ph.D. degree from Fudan University, China, in 2010. She was a Postdoctoral Fellow with the School of Information Science and Technology, Tsinghua University, from June 2010 to June 2012. She is currently a Professor with the College of Physics and Optoelectronic Engineering, Shenzhen University. Her research interests include optical communication, microwave photonics, and structured light field regulation.

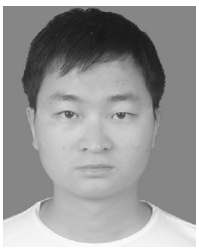

CHAOFENG WANG received the B.S. degree in optical information science and technology from Beijing Jiaotong University, China, in 2014. He is currently pursuing the master's degree with the Physics and Optoelectronic Engineering College, Shenzhen University. His research interest includes free-space optical communication.

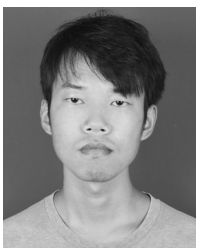

XIAOKE ZHANG received the B.S. degree in physics from the Hubei University of Arts and Science, China, in 2015. He is currently pursuing the master's degree with the Physics and Optoelectronic Engineering College, Shenzhen University. His research interest includes free-space optical communication.

JUNMIN LIU received the B.S. and M.E. degrees in computer science and technology from Hunan University, China, in 2010 and 2013, respectively. She is currently pursuing the Ph.D. degree with the Physics and Optoelectronic Engineering College, Shenzhen University. Her research interests include intelligent information processing and optical communication.

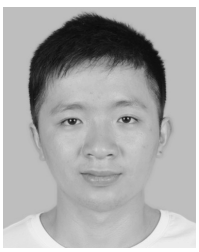

YANLIANG HE received the B.S. degree in optical information science and technology from East China Jiaotong University, China, in 2015. He is currently pursuing the Ph.D. degree with the Physics and Optoelectronic Engineering College, Shenzhen University. His research interest includes structured light field regulation.

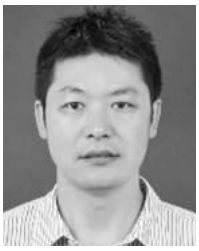

JIANGNAN XIAO received the Ph.D. degree from Hunan University, in 2014. In 2017, he joined the Shanghai Key Laboratory of Modern Optical System, Terahertz Technology Innovation Research Institute, University of Shanghai for Science and Technology, as a Lecturer. His research interests include wireless communication, optical fiber communication, optical wireless communication, and high-speed signal processing.

YANXIA GAO received the Ph.D. degree from the Chinese Academy of Sciences. In 1999, she joined Shenzhen University. She is currently a Professor. Her research interests include nonlinear optics, ultra-intense laser, ultra-short pulse optics, and ultra-short pulse optical communication.

SHUQING CHEN received the Ph.D. degree from Hunan University, China, in 2015. In September 2015, he joined the 2D Materials Optoelectronic Technology International Cooperation Joint Laboratory, Shenzhen University, as an Assistant Professor. His research interests include high-speed optical communication technology, optical wireless technology, visible light communication technology, intelligent information processing, and all-optical information devices.

XIAOMIN ZHANG graduated from the Department of Optics, Shandong University, in January 1982. After graduation, he is engaged in long-term research work on high-power solid-state laser technology and engineering. He is also a member of the China Optical Association and the Deputy Director of the China Academy of Engineering Physics.

DIANYUAN FAN graduated from the Physics Department, Peking University, in 1962. In 1966, he studied at the Institute of Electronics, Chinese Academy of Sciences, and the Shanghai Institute of Optics and Mechanics. After graduation, he worked at the Shanghai Institute of Optics and Fine Mechanics, Chinese Academy of Sciences. In 1995, he was elected as an Academician of the Chinese Academy of Engineering. He is currently a Laser Technology and Engineering Expert, an Academician of the Chinese Academy of Engineering, a Researcher with the Shanghai Institute of Optics and Fine Mechanics, Chinese Academy of Sciences, and the Director of the 2D Materials Optoelectronic Technology International Cooperation Joint Laboratory, Shenzhen University.